#### Research

# Subseasonal variability of ocean currents in the Bay of Bengal

Bradford S. Barrett<sup>1</sup> · Alexander R. Davies<sup>2</sup> · Cody P. Spedero<sup>3</sup> · Nadim Mahmud<sup>4</sup> · Joseph P. Smith<sup>2</sup> · Md. Masud-Ul-Alam<sup>4,5</sup> · Md. Hanif Biswas<sup>6</sup> · Md. Kawser Ahmed<sup>7</sup>

Received: 25 December 2024 / Accepted: 17 September 2025

Published online: 25 September 2025 © The Author(s) 2025 OPEN

#### **Abstract**

Upper-ocean currents in the Bay of Bengal (BoB) reverse seasonally in response to wind forcing. Less is known about their behavior on the subseasonal (30–60-day) time scale, including by phase of the leading mode of subseasonal atmospheric variability in the tropics, the Madden-Julian Oscillation (MJO). In this study, anomalies of National Aeronautics and Space Administration (NASA) Ocean Surface Current Analysis Real-time (OSCAR) upper-ocean zonal and meridional current components from 1993 to 2020 were composited by phase of the active MJO to examine how the upper-ocean currents vary subseasonally. These ocean current anomalies were then correlated with anomalies of 10-m zonal and meridional wind from the European Centre for Medium-Range Weather Forecasts (ECMWF) 5th Generation Reanalysis (ERA5) to quantify their relationship to the MJO. The strongest correlations between anomalies of upper-ocean currents and surface winds were found when the active MJO was over Africa (in phase 1) during September and October. In that phase, the BoB south of 10° N sees a reduction in zonal currents by as much as - 0.6 standard anomalies. Other important correlations between anomalies of ocean currents and surface winds were found when the active MJO is over the western Pacific (in phase 6) during September and October, over the Indian Ocean (in phase 2) during November and December, and over the Maritime Continent (in phase 4) during January and February. During the summer monsoon months of May to August, no MJO phases had correlations stronger than + 0.3 between anomalies of upper-ocean currents and surface winds. These results highlight the potential importance of the MJO in subseasonal ocean prediction and motivate future work to better understand the processes by which the MJO modulates the upper ocean.

### 1 Introduction

Ocean currents in the Bay of Bengal (BoB) are dynamic and respond strongly to seasonal wind forcing from the South Asian Monsoon [1–5]. During the summer monsoon, near-surface winds over the entire BoB are primarily out of the southwest in response to pressure falls and strong ascent over South Asia [6]. During the winter monsoon, near-surface winds reverse and are primarily out of the northeast in response to strong pressure rises and descent over the continent [7]. Upper-ocean currents in the BoB mostly reflect this strong seasonality in wind patterns [8, 9], although Kelvin wave responses to the wind forcing lead to a complex series of seasonally reversing gyres [10]. During the summer monsoon, mean upper-ocean currents form a counter-clockwise gyre over the northern BoB [1, 5], with westward and southwestward flow along Bangladesh and the northeastern coast of India [11–13] and

Example 2 Bradford S. Barrett, bradford.barrett@gmail.com | ¹Air Force Office of Scientific Research-Retired, Raleigh, NC, USA. ²Department of Ocean and Atmospheric Sciences, U.S. Naval Academy, Annapolis, MD, USA. ³Naval Air Station Oceana, Virginia Beach, VA, USA. ⁴Department of Oceanography and Hydrography, Bangladesh Maritime University, Dhaka, Bangladesh. ⁵Skidaway Institute of Oceanography and Department of Marine Sciences, University of Georgia, Savannah, GA, USA. ⁶Bangladesh Oceanographic Research Institute, Ramu, Cox's Bazar, Bangladesh. ⁵Department of Oceanography, University of Dhaka, Dhaka, Bangladesh.



Discover Oceans (2025) 2:44

| https://doi.org/10.1007/s44289-025-00081-6



(2025) 2:44

eastward and northeastward flow in the center of the Bay along 15° N. Further south and off the coast of Sri Lanka, there is a prominent northeastward current that borders a gyre and broad eastward flow across the BoB south of 15° N. During the winter monsoon, the East Indian Coastal Current (EICC) flows on average northward and is part of two prominent clockwise gyres that develop in response to the wind field along the Indian and Sri Lankan coasts. These oceanic features tend to lag the strongest monsoon winds by about a month [14]. Along the equator, south of 10° N, mean wintertime currents are westward [11, 12]. On the western side of the basin, currents form a gyre system that transitions between monsoon seasons. On the eastern side of the basin, surface currents in the Andaman Sea follow the pattern of the greater BoB, with a single gyre with clockwise circulation in the winter and counterclockwise circulation during the summer, shifting direction in response to Kelvin wave dynamics [5, 11, 15] and wave breaking as wind-driven currents impinge upon land in the enclosed basin [16, 17]. The imparted kinetic energy on the ocean surface occurs via series of air-sea momentum exchanges, and these interactions can be particularly complex when the wind stress-induced friction is against the direction of the prevailing currents [18, 19] reviews many of these important wind-wave processes that occur on a range of spatial and temporal scales.

Despite this good understanding of the seasonal variability in ocean circulation in the BoB in response to seasonally varying surface winds, the subseasonal (from two weeks up to 60 days [20]) variability of ocean circulation in response to subseasonal variability in surface winds remains understudied [21, 22]. The leading mode of atmospheric subseasonal (also referred to as intraseasonal; see the review in [20]) variability in the tropics is the Madden–Julian Oscillation [23–27]. The MJO is defined by a region of enhanced convection that propagates eastward along the equator on time scales of 30–60 days. This region of anomalously enhanced convection is preceded and followed by areas of anomalously suppressed convection. The MJO has been shown to modulate surface winds via an adjustment to surface pressures in response to vertical circulations that result from diabatic heating-driven divergence in the upper troposphere [27]. This modulation of surface winds is direct in the tropics [23, 24] and via a Rossby wave response in the extratropics [25, 27], and it extends many thousands of kilometers from the equator [27, 28]. Convective anomalies of the MJO thus control local patterns in sea-level pressure [28], with anomalous low pressure located in the region of upper-troposphere divergence and anomalous high pressure located in the regions of upper-troposphere convergence. These pressure anomalies, in turn, exert significant control on surface winds [29] and even precipitation in both the tropics [30] and beyond [31, 32]. Indeed, these links between MJO convection and surface winds and between surface winds and upper-ocean currents form the core of the physical mechanism for MJO modulation of upper-ocean currents in the BoB studied here. It is important to note that other modes of subseasonal atmospheric variability are active in the Indian Ocean and BoB, especially in summer, including the Indian monsoon intraseasonal oscillation (MISO [33]) and the Boreal Summer Intraseasonal Oscillation (BSISO [34]). Moreover, it is important to note that ocean circulation in the BoB is significantly modulated by the remote-forcing of equatorial MJO winds via the Kelvin wave dynamics discussed above and summarized in [59]. However, the analyses in this study are limited to the MJO and direct forcing from its wind anomalies in the BoB.

Modulation of lower-tropospheric circulation over the tropical oceans on the subseasonal time scale has been known and understood for more than 50 years [35]. Additionally, ocean circulation response to wind forcing has been known for more than 70 years [36]. What remains less understood is how that wind modulation may project onto surface ocean currents on the subseasonal time scale. A few studies have explored this link, finding MJO-driven subseasonal variability of the California current [37], the Leeuwin current off western Australia [28], sea levels across the equatorial Pacific [38], and currents off the coast of South Vietnam [6]. In the Indian Ocean, the West India Coastal Current (WICC) has been found to exhibit bursts of subseasonal variability [39], and subseasonal breaks in the southwest monsoon have been shown to affect sea-surface temperatures in the BoB [22, 39, 40]. Wind stress forcing on the subseasonal time scale has been observed to generate anomalies in sea surface height in the Indian Ocean up to 10 cm that travel throughout the basin, including into the BoB and Andaman Sea [41]. Given these findings, the BoB presents an opportunity to further explore how the MJO modulates surface ocean currents on the subseasonal time scale. This is possible because the upper ocean responds to wind forcing, particularly at low latitudes [22, 39, 40]. In this study, we examine subseasonal variability of upper-ocean currents in the BoB concurrent with subseasonal variability of surface winds. While ocean influences on the MJO have been documented (eg, [43]), less is known about how ocean currents in the BoB are modulated by the MJO. The remainder of this paper is organized as follows: data sets and analysis methods are described in Sect. 2, results of the MJO modulation of atmospheric and oceanic processes are presented in Sect. 3, and finally conclusions from this study are offered in Sect. 4.



#### 2 Data and methods

## 2.1 Study area

In this study, the BoB is defined as the basin area north of 5° N, to include the Andaman Sea (Fig. 1). The BoB is bounded to the west by the Indian subcontinent and Sri Lanka, to the north by Bangladesh and the Ganges River basin, and to the east by Burma and the Andaman Island chain. The focus here is on ocean currents in the upper 30 m in the region bounded by the features listed above.

## 2.2 Subseasonal variability: the Madden-Julian Oscillation

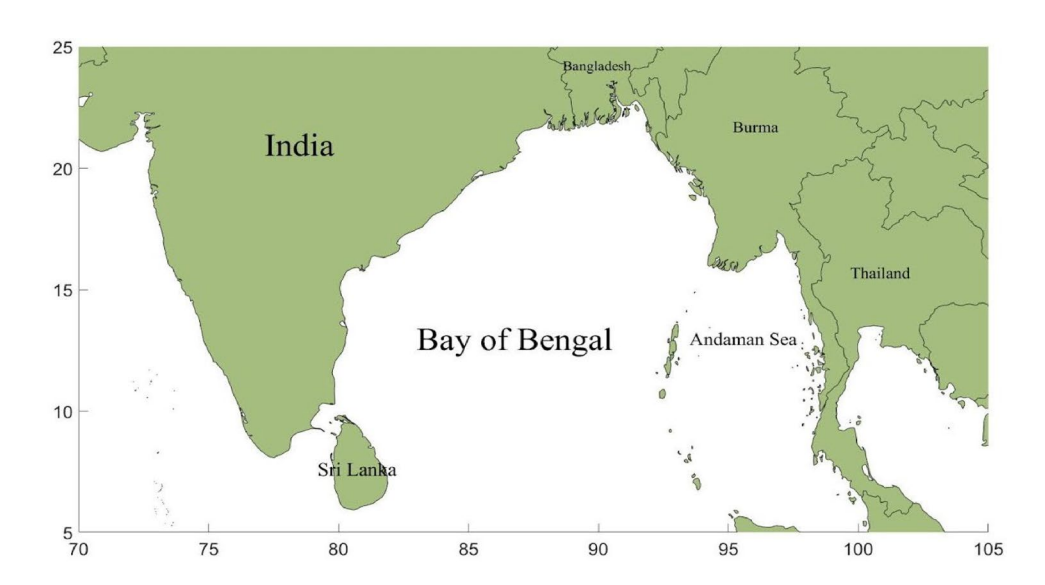
The amplitude and phase of the MJO were determined using the Real-time Multivariate MJO (RMM) index [44], which is available at daily time resolution from 1973 to present from http://www.bom.gov.au/climate/mjo/. The RMM index is created via an empirical orthogonal function analysis of 200-hPa zonal winds, 850-hPa zonal winds, and outgoing long-wave radiation (OLR) averaged across the tropics (15° S to 15° N) along the equator. The RMM index has the seasonal signal removed via a 20–100-day bandpass filter [44]. An active MJO event is defined in this study following [45] as one with an amplitude (RMM1² + RMM2²)<sup>0.5</sup> greater than or equal to 1.0, with RMM1 and RMM2 defined as the first two principal components of the empirical orthogonal function analysis [44]. This method of using the RMM to define the MJO is common in studies of subseasonal variability across all seasons [46–48].

#### 2.3 Ocean currents

Ocean currents analyzed in this study are from the National Aeronautics and Space Administration (NASA) Ocean Surface Current Analysis Real-time (OSCAR) data product. The OSCAR product provides gridded, 5-day (pentad) averaged zonal (u) and meridional (v) components for the upper 30 m of the ocean at 1/3° resolution [49] from 1993 to present. OSCAR currents are derived from measurements of sea surface height, surface vector wind, and sea surface temperature. Currents are calculated from those based on geostrophy, Ekman and Stommel wind stress dynamics, and the surface buoyancy gradient [49]. In this study, the OSCAR currents were analyzed from 01 January 1993 to 31 December 2020, stopping in 2020 to avoid the change in temporal and spatial resolution that took effect in 2021 [50].

Zonal and meridional current components were grouped by month pairs: January–February, March–April, May–June, July–August, September–October, and November–December, following [11] and the climatological analyses of [1, 2]. Pentad anomalies of the *u* and *v* components were calculated by subtracting the long-term (1993–2020) average for each month pair. The surface current anomalies were then binned by the active phase of the RMM index averaged over the pentad coincident with the OSCAR data. To capture direct impacts from the MJO, no time lag was considered, following [51]. The surface current anomalies were converted to standard anomalies by dividing each by the long-term

**Fig. 1** Area of focus for this study





standard deviation for each month pair [52]. Statistical significance of the mean standard anomaly for each MJO phase for each month pair was calculated following [37] using the two-sample t test. The t statistic was calculated for the u and v components as follows:

$$t = \frac{\overline{x} - \overline{y}}{\sqrt{\frac{s_x^2}{n} + \frac{s_y^2}{m}}}$$

where  $\bar{x}$  is the mean anomaly for each month pair,  $\bar{y}$  is the mean anomaly for each MJO phase,  $s_v^2$  and  $s_v^2$  are the corresponding standard deviations of each sample, and *n* and *m* are the sizes of each sample.

### 2.4 Surface winds

Zonal (U) and meridional (V) 10-m wind components analyzed in this study are from the European Centre for Medium-Range Weather Forecasts (ECMWF) 5th Generation Reanalysis (ERA5) [53]. The ERA5 product is available hourly at 0.25° grid spacing from January 1940 to present. In this study, daily values at 0000 UTC from 01 January 1993 to 31 December 2020 were analyzed. To avoid confusion, surface ocean current components are referred to hereafter using lower-case notation (u and v) and atmospheric wind components are referred to using upper-case notation (U and V). The 10-m wind components were pentad-averaged to coincide with the dates of the OSCAR surface currents, and similar to the OSCAR data, binned by MJO phase and month pairs. Standard anomalies were calculated following the method used for the ocean currents (see Sect. 2.3). Statistical significance of the standard anomalies of the surface winds was also calculated using the two-sample t-test. Other than the bandpass filter applied to the RMM index to remove seasonal variability, no other detrending of the data used in this study was done.

## 2.5 Subseasonal relationships: ocean currents and surface winds

The strength of the agreement between anomalies of ocean currents and anomalies of surface winds was quantified via Pearson product-moment correlation coefficients. Correlation coefficients at every grid point in the BoB were calculated between u and U and v and V for each MJO phase and month pair. To calculate these correlations, the atmospheric anomalies were re-gridded onto the OSCAR latitude-longitude grid. Correlations of at least moderate strength (0.3 < |r| < 0.6, following [52]) were selected for further analysis. It is important to note that due to the large number of paired gridded observations (n > 400) used to calculate these correlations in the BoB, coefficients r larger than 0.30 are statistically significant beyond 99.9% (p < 0.001).

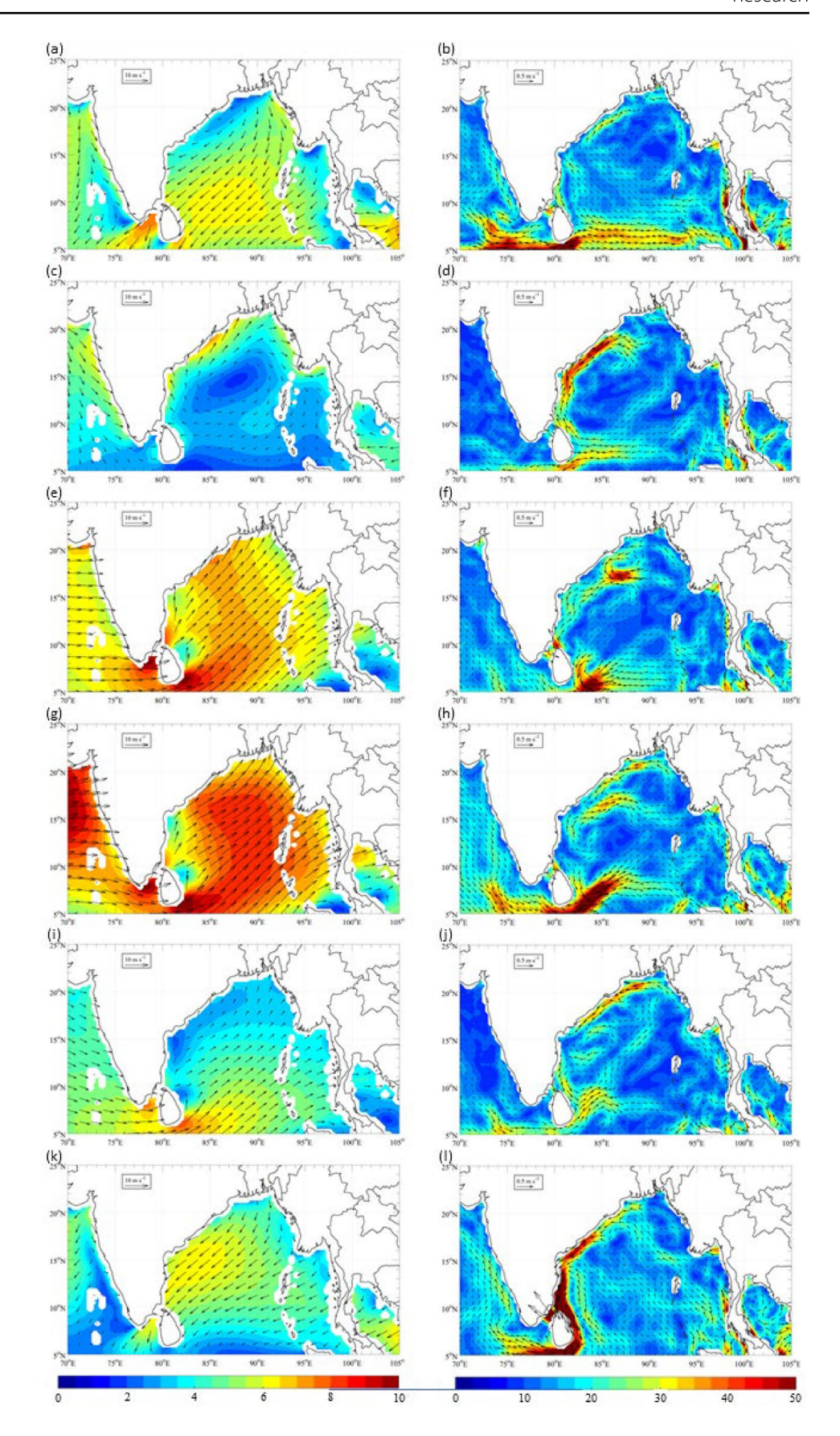
#### 3 Results

## 3.1 Climatology of ocean currents and surface winds

To understand potential subseasonal variability in the BoB, it is necessary to first examine the mean climatological state. Average ocean currents and surface winds for the six two-month periods of this study are presented in Fig. 2. In January-February, mean surface winds are uniformly from the northeast over much of the Bay at speeds between 5 and  $7 \text{ m s}^{-1}$  (Fig. 2a). The most prominent upper-ocean features in the BoB include a clockwise gyre over the northern half of the Bay at speeds of 5–25 cm s<sup>-1</sup>, a southward flowing current along southeastern India at speeds up to 20 cm s<sup>-1</sup>, and westward flow between 5° and 10° N up to 40 cm s<sup>-1</sup> (Fig. 2b). In March–April, surface winds are anti-cyclonic, with strongest winds along the east coast of India (Fig. 2c). In the ocean, the northward-flowing EICC is pronounced along the eastern coast of India at speeds approaching 50 cm s<sup>-1</sup>. The EICC forms the western part of a clockwise gyre over the western Bay (Fig. 2d). Westward flow is still present between 5° and 10° N but at speeds of 15–25 cm s<sup>-1</sup>, weaker than in January-February. In May-June, surface winds over the BoB are mostly from the southwest at speeds between 5 and 7 m s $^{-1}$ , reflecting the seasonal shift from winter, with exceptions in the northern lee of Sri Lanka (variable directions with speeds less than 3 m s<sup>-1</sup>) and the southern lee of Sri Lanka (winds from the southwest with speeds exceeding 8 m s<sup>-1</sup>) (Fig. 2e). The most prominent ocean features are cyclonic gyres of approximately 500 km in diameter, one east of India along 17° N and the other east of Sri Lanka along 7° N (Fig. 2f). Flows in those gyres approaches 50 cm s<sup>-1</sup>. Currents in the southern



Fig. 2 Mean 10-m winds (in m s<sup>-1</sup>) and currents in the upper 30 m of the ocean (in cm s<sup>-1</sup>) for **a, b** January–February, **c, d** March–April, **e, f** May–June, **g, h** July–August, **i, j** September–October, and **k, l** November–December, respectively. Winds are from the ERA5 reanalysis and ocean ocean currents are from the OSCAR product, both averaged over 1993–2020





BoB between 5°-10° N have reversed direction compared to January-April and are now eastward. In July-August, mean surface winds in July-August in the BoB are uniformly from the southwest between 7 and 9 m s<sup>-1</sup>, except to the east of Sri Lanka where they exceed 10 m s $^{-1}$  (Fig. 2q). In the ocean, a pronounced counterclockwise gyre is located over much of the northern Bay north of 15° N with fastest speeds exceeding 30 cm s<sup>-1</sup> along the India-Bangladesh border. Some of the fastest flow of the year in the BoB is found in July-August to the east of Sri Lanka, with speeds exceeding 50 cm s<sup>-1</sup> (Fig. 2h). Mean surface winds in September-October remain from the southwest, but unlike May-August, speeds are lower, only 2-6 m s<sup>-1</sup>, fastest in the lee side of Sri Lanka (Fig. 2i). Surface ocean currents in September-October are more complex than in other months (Fig. 2j). The EICC flows southward between 10-40 cm s<sup>-1</sup>, with fastest flow south of the Ganges River delta. It forms the western part a broad clockwise gyre in the northern BoB and a smaller clockwise gyre along 10° N. Sandwiches between these two is an anticlockwise gyre along 15° N. Surface currents converge east of Sri Lanka and progress to the east (Fig. 2i). Surface winds in November–December are generally from the north and northeast at speeds between 3 and 6 m s<sup>-1</sup> (Fig. 2k). Surface ocean currents in the BoB are dominated by a strong southwardflowing EICC, with speeds exceeding 50 cm s<sup>-1</sup> between 5° and 15° N (Fig. 2I). Over the remainder of the Bay, surface flow is mostly from southeast to northwest at speeds up to 20 m s $^{-1}$ .

## 3.2 Correlations between ocean currents and surface winds

Correlation coefficients were calculated between two sets of component anomalies: the zonal ocean currents (u) and zonal surface winds (U) and the meridional ocean currents (v) and meridional surface winds (V). These correlations were calculated for each month pair and MJO phase and reveal the several important aspects of the subseasonal modulation of the upper ocean in the BoB by the surface wind field (Table 1). First, the strongest relationships between the subseasonal wind anomalies and the subseasonal upper-ocean current anomalies are found in phase 1 in September-October in the zonal direction (r=0.37), in phase 6 also in September–October in the zonal direction (r=0.34), in phase 2 in November–December in the zonal direction (r = 0.33), and in phase 4 in January–February in the meridional direction (r=0.31). Second, the strongest correlations are all positive, indicating a direct relationship between subseasonal wind anomalies and subseasonal ocean current anomalies. Third, the strongest relationships between subseasonal winds and subseasonal ocean currents cluster in the months from September to February, outside of the summer monsoon. Fourth, the strongest relationships between subseasonal winds and subseasonal ocean currents appear to be in the zonal direction, although the strongest correlation coefficient in January-February is in the meridional direction. To further understand these results, composite anomalies for the four strongest phase-month pairs are examined in more detail.

### 3.3 Strongest relationships between ocean currents and surface winds

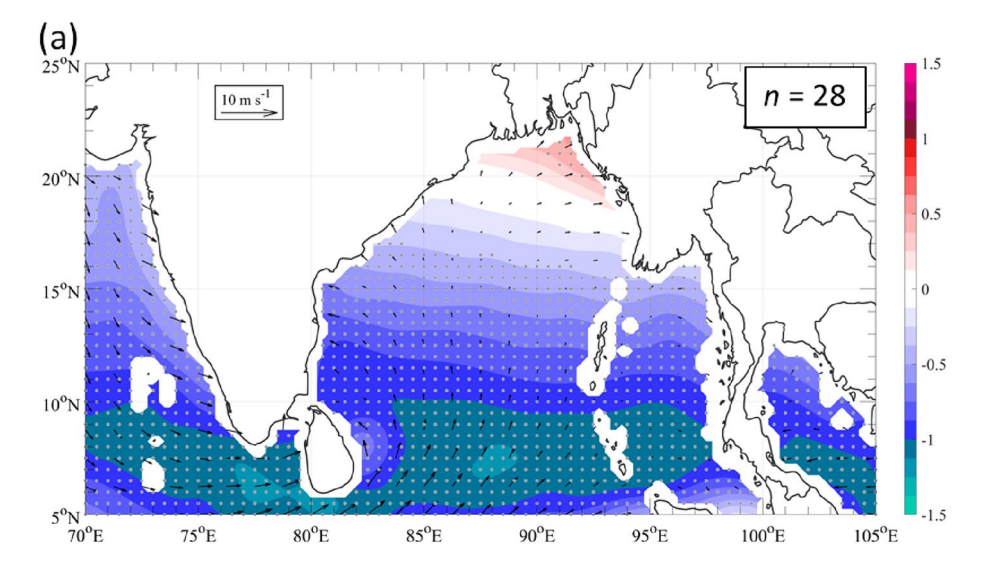
In September-October days in phase 1, the average zonal component of surface wind is anomalously negative throughout nearly the entire BoB south of 18.5° N (Fig. 3a). The strongest zonal anomalies, up to -1.5 standard anomalies, are located in the southern BoB between 5° and 10° N. Positive zonal wind anomalies, up to +0.3 standard anomalies, are located in the extreme northern BoB adjacent to Bangladesh. At the same time, negative zonal current anomalies, up to

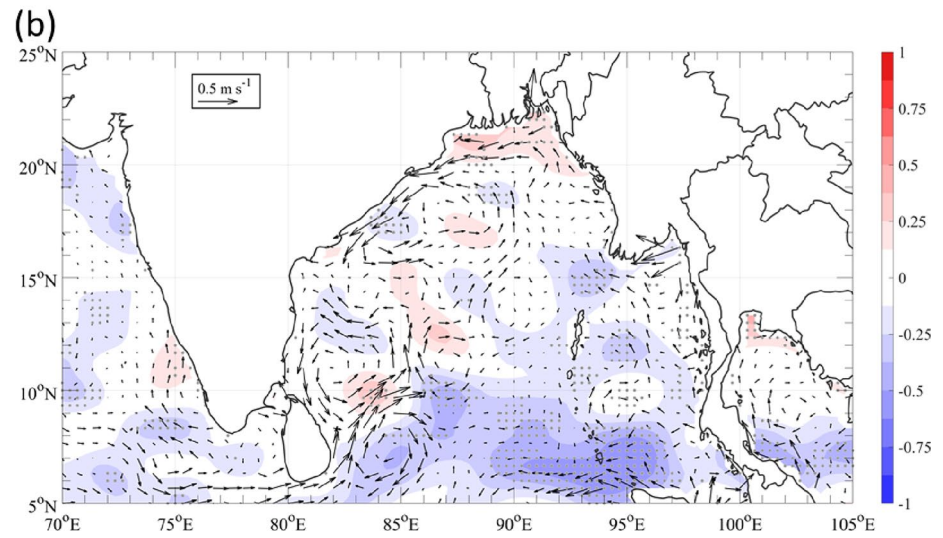
Table 1 Pearson productmoment correlation coefficients r between 10-m wind anomalies and upperocean current anomalies over the Bay of Bengal between 77 and 94° E and 5-25° N. Bolded values indicate moderate correlations (defined as 0.3 < |r| < 0.6, following [52]

		Phase 1	Phase 2	Phase 3	Phase 4	Phase 5	Phase 6	Phase 7	Phase 8
Jan–Feb	Zonal	0.06	- 0.09	0.04	0.01	- 0.06	0.25	0.03	0.15
	meridional	-0.03	-0.02	0.08	0.31	0.13	0.16	0.04	0.23
Mar–Apr	Zonal	0.03	0.09	0.18	-0.10	- 0.05	- 0.01	0.06	0.04
	meridional	- 0.19	- 0.07	- 0.11	-0.06	0.03	0.04	- 0.06	0.20
May–Jun	Zonal	0.01	0.01	- 0.10	- 0.03	- 0.05	0.17	0.02	0.06
	meridional	0.04	-0.03	0.10	0.13	0.00	80.0	- 0.12	0.01
Jul-Aug	Zonal	0.29	0.13	0.03	0.11	0.20	0.07	0.22	0.18
	meridional	0.01	0.15	- 0.06	- 0.11	0.13	0.20	0.11	- 0.10
Sep-Oct	Zonal	0.37	0.26	- 0.07	0.16	0.27	0.34	0.23	- 0.07
	meridional	0.15	- 0.03	0.04	0.08	0.04	0.09	0.12	0.06
Nov-Dec	Zonal	0.19	0.33	- 0.01	- 0.11	0.04	0.03	0.06	- 0.18
	meridional	0.10	0.06	0.17	- 0.06	0.04	0.20	- 0.08	- 0.08



Fig. 3 a Mean 10-m winds (vectors, in m s<sup>-1</sup>) and zonal standard anomalies (color shading, in units of standard anomalies), from the ERA5 reanalysis for days in September-October in active MJO phase 1. b Mean upperocean (upper 30 m) currents (vectors, in m s<sup>-1</sup>) and zonal standard anomalies (color shading, in units of standard anomalies) from the OSCAR data product for days in September-October in active MJO phase 1. Sample size (n) indicates number of 5-day pentads in each composite average, and stippling in both panels indicates zonal anomalies statistically significant at the 95th percentile



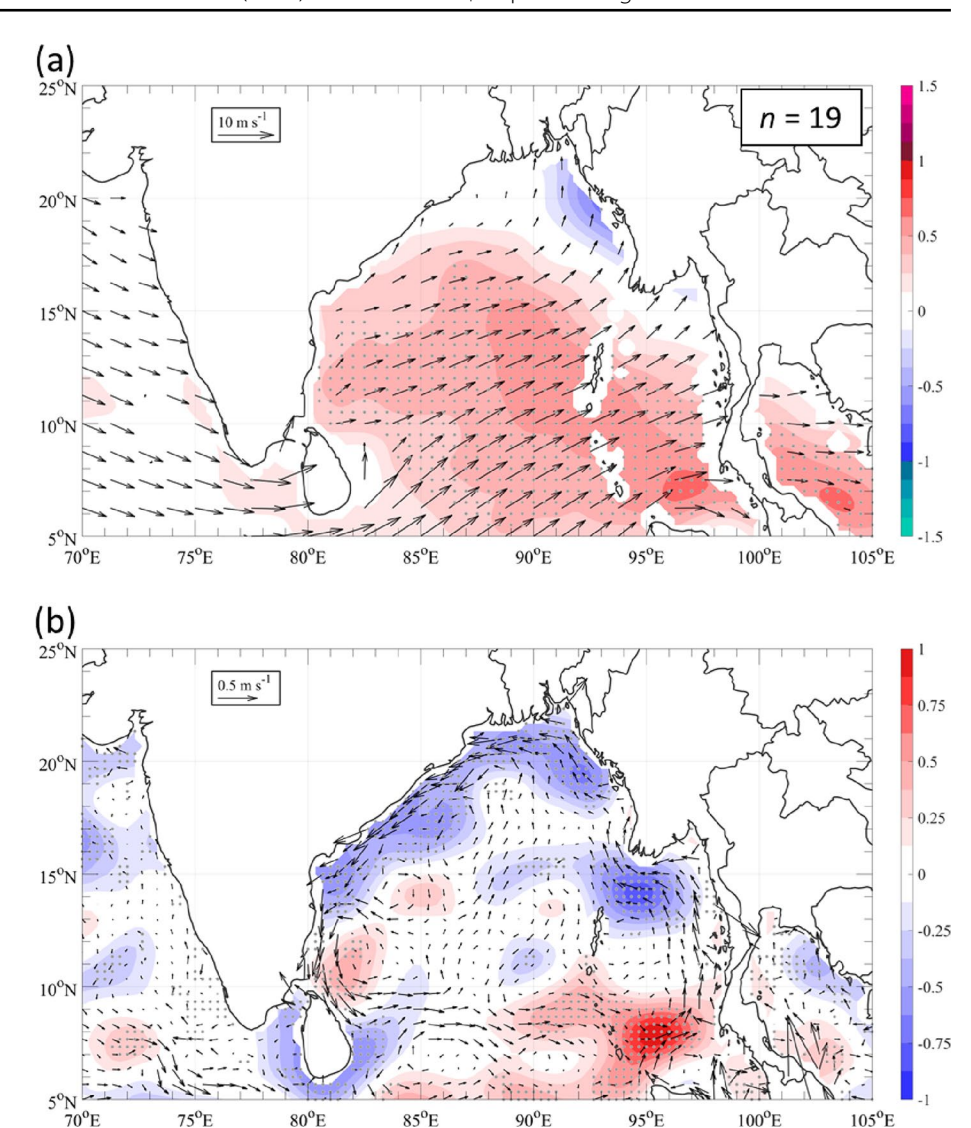


- 0.5 standard anomalies, are located over the southern BoB, especially south of 12° N and east of 85°E (Fig. 3b). Positive zonal current anomalies, up to +0.3 standard anomalies, are found in the extreme northern portions of the BoB, north of 20° N. The co-location of negative zonal wind anomalies with negative zonal current anomalies, and positive zonal wind anomalies with positive zonal current anomalies, yields a moderate correlation between the two (r=0.37). Physically, this is interpreted to indicate that on September–October days when the MJO is active and in phase 1, the southwesterly winds in the southern two-thirds of the BoB (south of 17.5° N) are weaker than average (Fig. 2i). The OSCAR derived currents in the southernmost portion of the BoB are modulated to favor a more westerly zonal component in a statistically significant way. While the exact reason is beyond the scope of this observational paper, based on how the OSCAR currents are derived [49], it is possible this is due to changes in surface geostrophic or Ekman processes associated with a more northward component of the wind vectors in Fig. 3a compared with Fig. 2i. In addition, the OSCAR current anomaly shows a stronger eastward modulation in the surface current along the northern part of the BoB. However, the overall southward flow of the EICC remains.

In September–October days in phase 6, the mean zonal wind anomaly is positive, up to +0.6 standard anomalies, over the BoB south of 20° N (Fig. 4a). At the same time, positive anomalies of zonal surface currents, up to + 0.8 standard anomalies, are located over the southern third of the BoB (south of 10° N), particularly in the southeastern part in the And  $\frac{1}{2}$  A northern BoB, particularly in the northern Andaman Sea, along the coast of Bangladesh, and in the EICC. The general co-location of positive zonal wind anomalies with positive zonal ocean anomalies, and negative zonal wind anomalies with negative zonal ocean anomalies, supports a correlation r of +0.34. The physical interpretation is that there are



Fig. 4 As in Fig. 3, but for days in September-October in active MJO phase 6

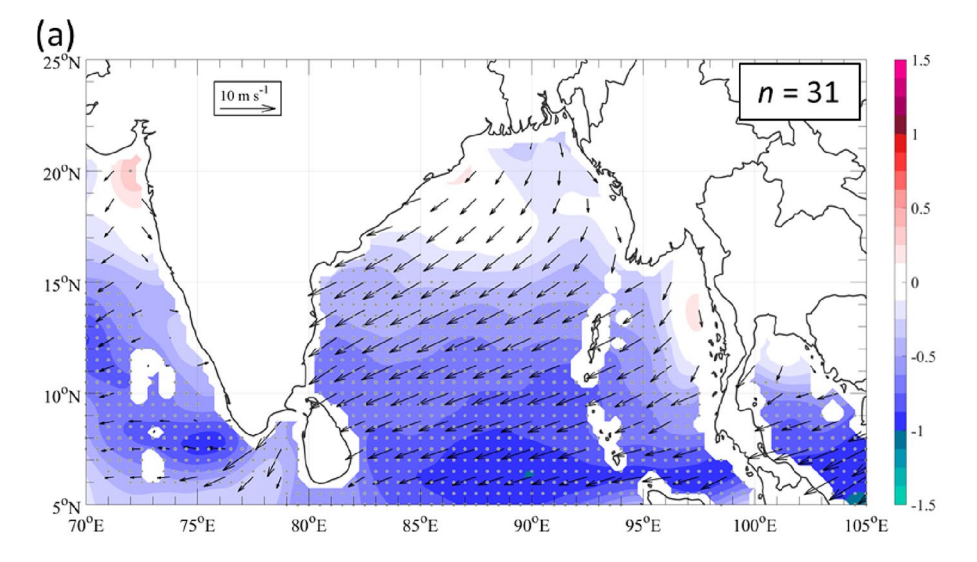


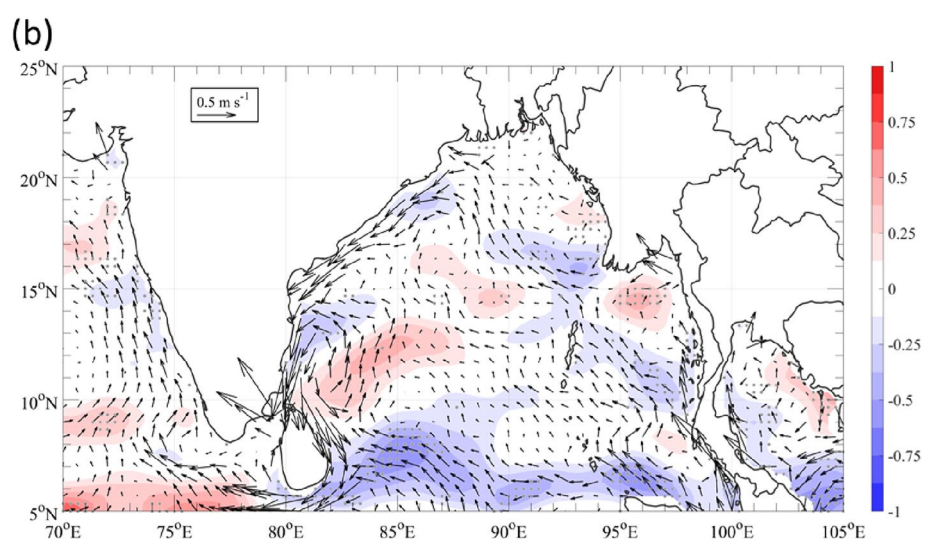
enhanced westerly winds over the majority of the basin on days in September-October when the MJO is active and in phase 6. This wind forcing enhances the counterclockwise circulation throughout the basin. This is evident in Fig. 4b through the southward enhancement of the EICC on the western edge of the basin, enhanced westward currents in the northern Andaman Sea, and enhancement in the eastward currents in the southeast position of the BoB and southern Andaman Sea. The meridional surface currents (not shown) show a similar pattern with an enhancement of the northward currents along the coast of Burma and a strengthening of the EICC. The exact mechanisms by which the changes in the wind forcing are modulating the surface currents during MJO active phase 6 in September and October are beyond the scope of this observational study and warrant further research. However, we hypothesize that the strengthened westerly wind forcing modulates the sea surface heights throughout the basin, which through geostrophy, projects onto existing the basin-wide currents.

In November-December days in phase 2, mean zonal wind anomalies are negative, up to -0.8 standard anomalies, over the southern three-fourths of the BoB, with the strongest anomalies between 5° and 10° N (Fig. 5a). The mean zonal current anomalies there are less uniform, with the strongest negative values, up to - 0.5 standard anomalies, over the southwestern BoB to the east of Sri Lanka (Fig. 5b). Other regions of negative zonal current anomalies are found in the southern and central Andaman Sea and along the northern and southern EICC. A region of positive zonal current anomalies, up to +0.4 standard anomalies, is found on the eastern side of the anti-clockwise gyre to the north of Sri Lanka. This more mixed pattern of zonal current anomalies co-located with a more uniform pattern of zonal wind anomalies results in a correlation between the two of r = 0.33. The physical interpretation is that on November–December days when the MJO is active and in phase 2, there is a statistically significant increased easterly component to the wind over most of



**Fig. 5** As in Fig. 3, but for days in November–December in active MJO phase 2



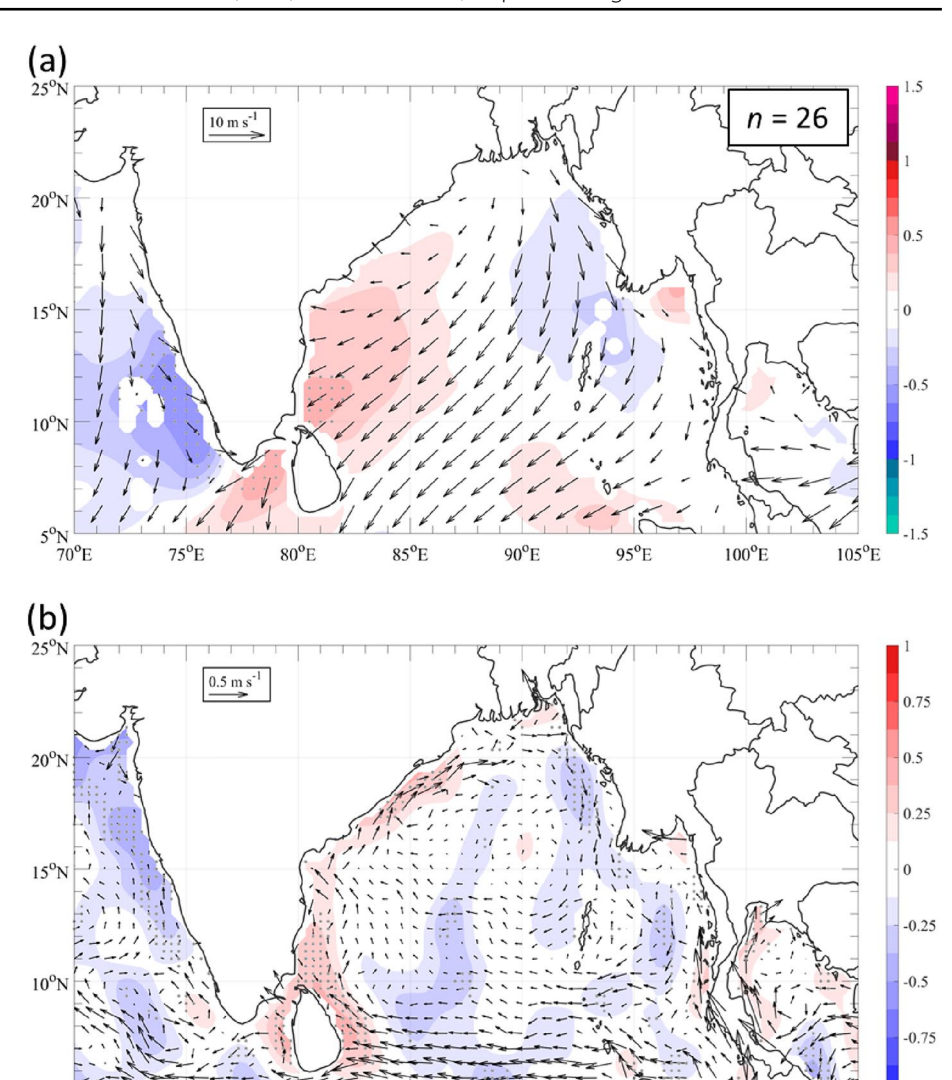


the basin. However, the current response is more muted. It is possible this is due to the strong EICC during these months that could overwhelm any smaller magnitude modulation from the MJO. Nevertheless, there is a coherent, although not uniformly statistically significant, modification to the circulation in the anti-clockwise gyre north of Sri Lanka is stronger, with -u anomalies on its northwestern side and +u anomalies on its southeastern side.

In January–February days in phase 4, meridional wind anomalies are oriented in an east–west dipole over the BoB. Positive meridional wind anomalies, up to +0.5 standard anomalies, are located over the western Bay and negative meridional wind anomalies, up to -0.35 standard anomalies, are found over the eastern Bay (Fig. 6a). The net result is a cohert pattern of weaking southwesterly flow over the basin compared to Fig. 2a which, although not statistically significant, is also supported by the zonal wind anomalies (not shown). At the same time, positive meridional current anomalies, up to +0.5 standard anomalies, are found in the far western portions of the Bay and negative meridional current anomalies, up to -0.3 standard anomalies, are found in the eastern Bay (Fig. 6b). The co-location of positive meridional ocean anomalies with positive meridional wind anomalies, and negative meridional ocean anomalies with negative meridional wind anomalies, is the primary reason for the moderate correlation (r=0.31) between the two. Although not shown, there is strengthening in the eastward flowing current along the northern coast of the BoB. This suggests an enhancement of the clockwise currents along the coastline within the BoB. This means that on January–February days when the MJO is active and in phase 4, the EICC is stronger and more poleward-flowing than average (+v), and the flow over the eastern BoB - particularly the southward-flowing currents in the northeastern BoB - is also stronger than average (-v). While the exact dynamic reasons for this are beyond the scope of this observational study, we hypothesize that the weaking of the northeasterly wind over the basin could modulate sea surface heights, which projects onto the OSCAR ocean currents.



Fig. 6 As in Fig. 3, but for meridional winds and currents on days in January-February in active MJO phase 4



90°E

105°E

## 4 Conclusions

In this study, variability of upper-ocean currents in the Bay of Bengal was examined by phase of the leading mode of subseasonal atmospheric variability, the MJO. Subseasonal anomalies of surface winds from the ERA5 reanalysis for the month pairs of January-February, March-April, May-June, July-August, September-October, and November-December were correlated with subseasonal anomalies of ocean currents from the OSCAR data product to identify the months and MJO phases with the strongest relationships between the two. Moderate positive correlations (0.3 < r < 0.6) were found four times: in September–October in the zonal direction in phases 1 and 6, in November-December in the zonal direction in phase 2, and in January-February in the meridional direction in phase 4. No correlations stronger than + 0.3 were found in the summer monsoon season from May-August.

Subseasonal variability of the surface wind field in the BoB has been shown previously [27] as the envelope of convection of the MJO translates eastward from the Indian Ocean through the Maritime Continent to the western Pacific Ocean. The novel results from this current study are that the OSCAR surface ocean currents in the BoB may be modulated by the subseasonal wind forcing of the MJO, and therefore themselves vary or be modulated subseasonally. The strongest correlation coefficients found here subseasonally are similar in magnitude to correlations found seasonally between surface winds and sea surface height by [60, 61] (r = 0.3-0.7). The subseasonal modulation of the OSCAR currents by the MJO is not observed to be uniform; it depends on the MJO phase, month, and location in the basin.



While many processes can impact surface ocean currents, OSCAR currents are derived from geostrophy, Ekman and Stommel wind stress dynamics, and the surface buoyancy gradient [49]. Therefore, the physical interpretation of the OSCAR current modulation via variability in wind forcing by MJO phase is limited to only those processes. Given that the OSCAR currents are surface velocities derived from both geostrophic and ageostrophic components, it is important to note that the correlations reported here do not differentiate between Ekman and Stommel processes and SSH-induced variability.

Within that context, the physical interoperation of the MJO-driven subseasonal variability of ocean currents in the BoB can be summarized as follows.

- On days in September–October when the MJO is active and in phase 1, OSCAR derived surface currents over the BoB are modified in reverse from their mean zonal state. For example, the OSCAR derived currents in portions of the southern BoB become westward instead of eastward. More generally, the OSCAR ocean currents in the southernmost portion of the BoB are modulated to favor a more westerly, statistically significant zonal component. The OSCAR current anomalies are in response to significant zonal weakness in the southwest monsoon winds in September–October during MJO active phase 1.
- 2. On days in September–October when the MJO is active and in phase 6, mean OSCAR derived ocean currents in the BoB are, on average, zonally enhanced. The eastward-flowing currents in the southern BoB and the southern Andaman Sea are more eastward, the currents south of Bangladesh have a stronger westward component, and the EICC has a stronger southwestward component. These zonal circulation anomalies are in response to significant subseasonal strengthening of the zonal component of the southwest monsoon winds, and stand in sharp contrast with the subseasonal wind anomalies and ocean response during September–October days in phase 1.
- 3. On days in November–December when the MJO is active and in phase 2, the current response is more muted. It is possible this is due to the climatologically strong EICC during these months that could overwhelm smaller-magnitude modulation from the MJO. Nevertheless, there is an apparent modulation to the circulation in the anti-clockwise gyre north of Sri Lanka is stronger that could be in response to a subseasonally strengthened northeasterly monsoon.
- 4. On days in January–February when the MJO is active and in phase 4, the northward-flowing EICC is stronger, on average, as are the southward-flowing currents over the eastern portion of the BoB. These subseasonal current anomalies are in response to an east–west dipole pattern in meridional surface winds, with weaker northerly winds in the western BoB and stronger northerly winds in the eastern BoB.

It is important to note several considerations. First, statistically significant subseasonal variability of the OSCAR derived ocean currents in the BoB is present only outside of the summer monsoon. It is possible that during the summer monsoon, the seasonal wind forcing overwhelms any subseasonal signal from the MJO. It is also possible that in summer months, subseasonal variability of ocean currents may be associated with other oscillations (discussed below). However, those possibilities are beyond the scope of this study. Second, in the months with moderate correlations between subseasonal wind anomalies and subseasonal ocean anomalies, the relationship was only found in one directional component (zonal or meridional), and in three of the four instances, it was the zonal component that was modulated. The reason for this is unclear. Third, the magnitude of the correlation coefficients implies that subseasonal variability in the surface winds explains up to about 15% of the variability in the surface currents, suggesting that other wind wave processes [e.g., 20] or modes of variability may influence ocean circulation at those scales. Fourth, the OSCAR data product includes both the geostrophic and ageostrophic (simplified Ekman and Stommel) components [49]. It is unclear whether the MJO-driven surface wind projects more strongly onto one or the other, as the correlations reported here do not distinguish between the two processes.

Understanding subseasonal ocean variability has important practical applications. One application of these results is in forecasting, as the MJO now shows skillful prediction out to four weeks [58]. These results can help inform conceptual models that project into the subseasonal time period. Another application is to motivate future research. As this is one of the first studies to document a potential modification of the ocean currents over the BoB due to subseasonal wind forcing from the MJO, there are multiple possible directions for follow-on studies. For example, future work is needed to better refine the dynamic mechanisms linking subseasonal wind variability to subseasonal ocean current variability. In addition, future research can leverage these results and explore subseasonal variability of other processes in the BoB, such as biogeochemical responses to variability in circulation, as suggested by [42, 54, 55]. Additionally, work is needed to better understand subseasonal variability of currents in the BoB during the summer monsoon. Two indices designed to capture subseasonal atmospheric variability in summer, the MISO [33] and BSISO [56], should be considered. Future



Discover Oceans

work may also consider time lags, as the relationships presented here are direct (over the five-day period of the OSCAR observations). Modes of variability that predominate on longer time scales, particularly the Indian Ocean Dipole and the El Nino-Southern Oscillation in the atmosphere and other wave regimes in the ocean, could also be considered alongside the MJO, as that was outside the scope of his study. Finally, further insight into the subseasonal variability of upper-ocean currents could be gained through analysis of other data products, including ocean reanalysis (e.g., ORAS5, [57]) or the NASA OSCAR 2.0 product available at daily (instead of in pentad) temporal resolution.

Acknowledgements This work was partially supported by the Office of Naval Research Award N0001416WX01752 and the U.S. Naval Academy Office of Research and Scholarship.

Author contributions B.B. designed the study, co-led the writing, contributed to the data analysis, and led the manuscript editing: A.D. co-led the writing and data analysis, and contributed to the study design; C.S. co-led the data analysis and contributed to the writing; J.S. contributed to the study design and manuscript editing; M.A.contributed to the study design and manuscript editing; N.M. contributed to the study design and manuscript editing; H.B. contributed to the manuscript writing and editing; and K.A. contributed to the study design.

Funding Office of Naval Research, U. S. Naval Academy.

Data availability The RMM is available at http://www.bom.gov.au/climate/mjo/, the OSCAR surface currents at https://podaac.jpl.nasa.gov/ dataset/OSCAR\_L4\_OC\_INTERIM\_V2.0, and surface wind speed from https://cds.climate.copernicus.eu/.

Code availability Not applicable.

#### **Declarations**

Ethics approval and Consent to participate Not applicable Not applicable.

Consent for publication Not applicable.

Competing interests The authors declare no competing interests.

Open Access This article is licensed under a Creative Commons Attribution-NonCommercial-NoDerivatives 4.0 International License, which permits any non-commercial use, sharing, distribution and reproduction in any medium or format, as long as you give appropriate credit to the original author(s) and the source, provide a link to the Creative Commons licence, and indicate if you modified the licensed material. You do not have permission under this licence to share adapted material derived from this article or parts of it. The images or other third party material in this article are included in the article's Creative Commons licence, unless indicated otherwise in a credit line to the material. If material is not included in the article's Creative Commons licence and your intended use is not permitted by statutory regulation or exceeds the permitted use, you will need to obtain permission directly from the copyright holder. To view a copy of this licence, visit http://creativeco mmons.org/licenses/by-nc-nd/4.0/.

# References

- 1. Potemra JT, Luther ME, O'Brien JJ. The seasonal circulation of the upper ocean in the Bay of Bengal. J Geophys Res Oceans. 1991;96(C7):12667-83. https://doi.org/10.1029/91JC01045.
- Schott FA, McCreary JP. The monsoon circulation of the Indian Ocean. Prog Oceanogr. 2001;51(1):1–123. https://doi.org/10.1016/S0079-6611(01)00083-0.
- 3. Shankar D, Vinayachandran PN, Unnikrishnan AS. The monsoon currents in the north Indian Ocean. Prog Oceanogr. 2002;52(1):63–120. https://doi.org/10.1016/S0079-6611(02)00024-1.
- 4. Kay S, Caesar J, Janes T. 'Marine Dynamics and Productivity in the Bay of Bengal. Cham: Springer; 2018.
- 5. Pirro A, Fernando HJS, Wijesekera HW, Jensen TG, Centurioni LR, Jinadasa SUP. Eddies and currents in the Bay of Bengal during summer monsoons. Deep Sea Res Part II. 2020;172:104728. https://doi.org/10.1016/j.dsr2.2019.104728.
- 6. Liu X, Wang J, Cheng X, Du Y. Abnormal upwelling and chlorophyll-a concentration off South Vietnam in summer 2007. J Geophys Res Oceans. 2012. https://doi.org/10.1029/2012JC008052.
- 7. Wang L, Yuan X, Ting M, Li C. Predicting summer Arctic Sea Ice concentration intraseasonal variability using a vector autoregressive model. J Clim. 2016;29(4):1529-43. https://doi.org/10.1175/JCLI-D-15-0313.1.
- 8. Vinayachandran PN. Impact of physical processes on chlorophyll distribution in the Bay of Bengal. Indian Ocean Biogeochem Processes Ecol var. 2009. https://doi.org/10.1029/2008GM000705.
- Chakraborty A. Gangopadhyay A. Development of a high-resolution multiscale modeling and prediction system for Bay of Bengal, Part l: climatology-based simulations. Open J Mar Sci. 2016;06(01):145-76. https://doi.org/10.4236/ojms.2016.61013.
- 10. Chatterjee A, Shankar D, McCreary JP, Vinayachandran PN, Mukherjee A. Dynamics of Andaman sea circulation and its role in connecting the equatorial Indian Ocean to the Bay of Bengal. J Geophys Res Oceans. 2017;122(4):3200-18. https://doi.org/10.1002/2016JC012300.
- 11. Varkey MJ, Murty VSN, Suryanarayana A. Physical oceanography of the Bay of Bengal and Andaman Sea. Oceanogr Mar Biol Annu Rev. 1996;34:1-70.



(2025) 2:44

- 12. Sil S, Chakraborty A. Simulation of East India coastal features and validation with satellite altimetry and drifter climatology. Int J Ocean
- Clim Syst. 2011;2(4):279–89. https://doi.org/10.1260/1759-3131.2.4.279.
  Dandapat S, Chakraborty A, Kuttippurath J. Interannual variability and characteristics of the East India Coastal Current associated with Indian Ocean Dipole events using a high resolution regional ocean model. Ocean Dyn. 2018;68(10):1321–34. https://doi.org/10.1007/s10236-018-1201-5
- 14. Hacker P, Firing E, Hummon J, Gordon AL, Kindle JC. Bay of Bengal currents during the Northeast monsoon. Geophys Res Lett. 1998;25(15):2769–72. https://doi.org/10.1029/98GL52115.
- Sen R, Pandey S, Dandapat S, Francis PA, Chakraborty A. A numerical study on seasonal transport variability of the North Indian Ocean boundary currents using Regional Ocean Modeling System (ROMS). J Oper Oceanogr. 2022;15(1):32–51. https://doi.org/10.1080/17558 76X.2020.1846266.
- 16. Vinayachandran PN, Shetye SR, Sengupta D, Gadgil S. Forcing mechanisms of the Bay of Bengal circulation. Curr Sci. 1996;71:753–63.
- 17. Vinayachandran PN, Masumoto Y, Mikawa T, Yamagata T. Intrusion of the Southwest Monsoon Current into the Bay of Bengal. J Geophys Res Oceans. 1999;104(C5):11077–85. https://doi.org/10.1029/1999JC900035.
- 18. McPhaden MJ, Athulya K, Girishkumar MS, Orlić M. Ekman revisited: surface currents to the left of the winds in the Northern Hemisphere. Sci Adv. 2024. https://doi.org/10.1126/sciadv.adr0282.
- Sullivan PP, McWilliams JC. Dynamics of winds and currents coupled to surface waves. Annu Rev Fluid Mech. 2010. https://doi.org/10. 1146/annurev-fluid-121108-145541.
- 20. Vitart F, Robertson AW. The sub-seasonal to seasonal prediction project (S2S) and the prediction of extreme events. NPJ Clim Atmos Sci. 2018;1(1):3. https://doi.org/10.1038/s41612-018-0013-0.
- 21. Mukherjee A, et al. Observed seasonal and intraseasonal variability of the East India Coastal Current on the continental slope. J Earth Syst Sci. 2014;123(6):1197–232. https://doi.org/10.1007/s12040-014-0471-7.
- 22. McCreary JP, Shetye SR. Observations and dynamics of circulations in the North Indian Ocean. Singapore: Springer Nature Singapore; 2023. https://doi.org/10.1007/978-981-19-5864-9.
- 23. Madden RA, Julian PR. Detection of a 40–50 day oscillation in the zonal wind in the tropical pacific. J Atmos Sci. 1971;28(5):702–8. https://doi.org/10.1175/1520-0469(1971)028<0702:DOADOI>2.0.CO;2.
- 24. Madden RA, Julian PR. Description of global-scale circulation cells in the tropics with a 40–50 day period. J Atmos Sci. 1972;29(6):1109–23. https://doi.org/10.1175/1520-0469(1972)029%3c1109:DOGSCC%3e2.0.CO;2.
- 25. Madden RA, Julian PR. Observations of the 40–50-day tropical oscillation—a review. Mon Weather Rev. 1994;122(5):814–37. https://doi.org/10.1175/1520-0493(1994)122%3c0814:OOTDTO%3e2.0.CO;2.
- 26. Hong J-Y, Kim J-H, Park D-SR. Reexamination of the Madden–Julian oscillation effect on wintertime sea ice concentrations in the North Pacific. Atmosphere. 2019;11(1):7. https://doi.org/10.3390/atmos11010007.
- 27. Zhang C. Madden-Julian Oscillation. Rev Geophys. 2005. https://doi.org/10.1029/2004RG000158.
- 28. Marshall AG, Hendon HH. Impacts of the MJO in the Indian Ocean and on the Western Australian coast. Clim Dyn. 2014;42(3–4):579–95. https://doi.org/10.1007/s00382-012-1643-2.
- 29. Matthews AJ. Propagation mechanisms for the Madden-Julian Oscillation. Q J R Meteorol Soc. 2000;126(569):2637–51. https://doi.org/10.1002/qj.49712656902.
- 30. Tan H, Ray P, Barrett BS, Tewari M, Moncrieff MW. Role of topography on the MJO in the maritime continent: a numerical case study. Clim Dyn. 2020;55(1–2):295–314. https://doi.org/10.1007/s00382-018-4275-3.
- 31. Donald A, Meinke H, Power B, Wheeler M and Ribbe J. Forecasting with the Madden-Julian Oscillation and the applications for risk management. In: Proceedings of the 4th international crop science congress (ICSC 2004), 2004.
- 32. Benedict JJ, Randall DA. Observed characteristics of the MJO relative to maximum rainfall. J Atmos Sci. 2007;64(7):2332–54. https://doi.org/10.1175/JAS3968.1.
- 33. Suhas E, Neena JM, Goswami BN. An Indian monsoon intraseasonal oscillations (MISO) index for real time monitoring and forecast verification. Clim Dyn. 2013;40(11–12):2605–16. https://doi.org/10.1007/s00382-012-1462-5.
- 34. Lee J-Y, Wang B, Wheeler MC, Fu X, Waliser DE, Kang I-S. Real-time multivariate indices for the boreal summer intraseasonal oscillation over the Asian summer monsoon region. Clim Dyn. 2013;40(1–2):493–509. https://doi.org/10.1007/s00382-012-1544-4.
- 35. Zhang C. Madden–Julian oscillation: bridging weather and climate. Bull Am Meteorol Soc. 2013;94(12):1849–70. https://doi.org/10.1175/BAMS-D-12-00026.1.
- 36. Munk WH. On the wind-driven ocean circulation. J Meteorol. 1950;7(2):80–93. https://doi.org/10.1175/1520-0469(1950)007%3c0080: OTWDOC%3e2.0.CO;2.
- 37. Barrett BS, Davies AR, Rose JI. Wind-driven response of the upper ocean along the U.S. West Coast to tropical MJO convection. J Geophys Res Oceans. 2017;122(10):8196–207. https://doi.org/10.1002/2017JC013086.
- 38. Oliver ECJ, Thompson KR. Madden-julian oscillation and sea level: local and remote forcing. J Geophys Res Oceans. 2010. https://doi.org/10.1029/2009JC005337.
- 39. Chaudhuri A, et al. Observed variability of the West India Coastal Current on the continental shelf from 2010–2017. J Earth Syst Sci. 2021;130(2):77. https://doi.org/10.1007/s12040-021-01603-4.
- 40. Lighthill MJ. Dynamic response of the Indian Ocean to onset of the Southwest monsoon. Philos Trans R Soc Lond Ser A, Math Phys Sci. 1969. https://doi.org/10.1098/rsta.1969.0040.
- 41. Waliser DE, Murtugudde R, Lucas LE. Indo-Pacific Ocean response to atmospheric intraseasonal variability: 2. boreal summer and the intraseasonal oscillation. J Geophys Res Oceans. 2004. https://doi.org/10.1029/2003JC002002.
- 42. Chen G, Han W, Li Y, Wang D, Shinoda T. Intraseasonal variability of upwelling in the equatorial Eastern Indian Ocean. J Geophys Res Oceans. 2015;120(11):7598–615. https://doi.org/10.1002/2015JC011223.
- 43. DeMott CA, Klingaman NP, Woolnough SJ. Atmosphere-ocean coupled processes in the Madden-Julian oscillation. Rev Geophys. 2015;53(4):1099–154. https://doi.org/10.1002/2014RG000478.
- 44. Wheeler MC, Hendon HH. An all-season real-time multivariate MJO index: development of an index for monitoring and prediction. Mon Weather Rev. 2004;132(8):1917–32. https://doi.org/10.1175/1520-0493(2004)132%3c1917:AARMMI%3e2.0.CO;2.



- 45. Lafleur DM, Barrett BS, Henderson GR. Some Climatological Aspects of the Madden–Julian Oscillation (MJO). J Clim. 2015;28(15):6039–53. https://doi.org/10.1175/JCLI-D-14-00744.1.
- 46. Kiladis GN, et al. A comparison of OLR and circulation-based indices for tracking the MJO. Mon Weather Rev. 2014;142(5):1697–715. https://doi.org/10.1175/MWR-D-13-00301.1.
- 47. Liu J, Curry JA. Accelerated warming of the Southern Ocean and its impacts on the hydrological cycle and sea ice. Proc Natl Acad Sci. 2010;107(34):14987–92. https://doi.org/10.1073/pnas.1003336107.
- 48. Flatau M, Kim Y-J. Interaction between the MJO and polar circulations. J Clim. 2013;26(11):3562–74. https://doi.org/10.1175/JCLI-D-11-00508.1.
- 49. Bonjean F, Lagerloef GSE. Diagnostic model and analysis of the surface currents in the tropical Pacific Ocean. J Phys Oceanogr. 2002;32(10):2938–54. https://doi.org/10.1175/1520-0485(2002)032%3c2938:DMAAOT%3e2.0.CO;2.
- 50. Dohan k, The Ocean Surface Current Analyses-Real Time (OSCAR) System. PO.DAAC. 2022. https://doi.org/10.5067/OSCAR-25F20.
- 51. Zheng C, Chang EKM. The role of MJO propagation, lifetime, and intensity on modulating the temporal evolution of the MJO extratropical response. J Geophys Res: Atmos. 2019;124(10):5352–78. https://doi.org/10.1029/2019JD030258.
- 52. Wilks DS. Statistical Methods in the Atmospheric Sciences. Cambridge: Academic Press; 2005.
- 53. Hersbach H, et al. The ERA5 global reanalysis. Q J R Meteorol Soc. 2020;146(730):1999–2049. https://doi.org/10.1002/gj.3803.
- 54. Waliser DE, Murtugudde R, Strutton P, Li J. Subseasonal organization of ocean chlorophyll: prospects for prediction based on the Madden-Julian oscillation. Geophys Res Lett. 2005. https://doi.org/10.1029/2005GL024300.
- 55. Lobitz B, et al. Climate and infectious disease: Use of remote sensing for detection of *Vibrio cholerae* by indirect measurement. Proc Natl Acad Sci. 2000;97(4):1438–43. https://doi.org/10.1073/pnas.97.4.1438.
- 56. Kikuchi K. 'The Boreal Summer Intraseasonal Oscillation (BSISO): a review. J Meteorol Soc Jpn Ser II. 2021;99(4):2021–45. https://doi.org/10.2151/jmsj.2021-045.
- 57. Zuo H, Balmaseda MA, Tietsche S, Mogensen K, Mayer M. The ECMWF operational ensemble reanalysis –analysis system for ocean and sea ice: a description of the system and assessment. Ocean Sci. 2019;15(3):779–808. https://doi.org/10.5194/os-15-779-2019.
- 58. Shin NY, Kang D, Kim D, Lee JY, Kug JS. Data-driven investigation on the boreal summer MJO predictability. NPJ Clim Atmos Sci. 2024;7(1):248. https://doi.org/10.1038/s41612-024-00799-8.
- 59. Girishkumar MS, Ravichandran M, Han W. Observed intraseasonal thermocline variability in the Bay of Bengal. J Geophys Res: Oceans. 2013;118(7):3336–49. https://doi.org/10.1002/jgrc.20245.
- 60. Han W, Webster PJ. Forcing Mechanisms of Sea Level Interannual Variability in the Bay of Bengal. J Phys Oceanogr. 2002;32:216–39. https://doi.org/10.1175/1520-0485(2002)032%3c0216:FMOSLI%3e2.0.CO;2.
- 61. Akhter S, Qiao F, Wu K, Yin X, Chowdhury KA, Chowdhury NUMK. Seasonal and long-term sea-level variations and their forcing factors in the northern Bay of Bengal: a statistical analysis of temperature, salinity, wind stress curl, and regional climate index data. Dyn Atmos Oceans. 2021;95:101239. https://doi.org/10.1016/j.dynatmoce.2021.101239.

Publisher's Note Springer Nature remains neutral with regard to jurisdictional claims in published maps and institutional affiliations.

